Evolution of Near-surface Flows Inferred from High-resolution Ring-diagram Analysis

Richard S. Bogart, Charles S. Baldner

Stanford University, Stanford, CA 94305-4085, USA

and

Sarbani Basu

Yale University, New Haven, CT 06520, USA

ABSTRACT

Ring-diagram analysis of acoustic waves observed at the photosphere can provide a relatively robust determination of the sub-surface flows at a particular time under a particular region. The depth of penetration of the waves is related to the size of the region, hence the depth extent of the measured flows is inversely proportional to the spatial resolution. Most ring-diagram analysis has focused on regions of extent $\sim 15^\circ$ (180 Mm) or more in order to provide reasonable mode sets for inversions. HMI data analysis also provides a set of ring fit parameters on a scale three times smaller. These provide flow estimates for the outer 1% (7 Mm) of the Sun only, with very limited depth resolution, but with spatial resolution adequate to map structures potentially associated with the belts and regions of magnetic activity. There are a number of systematic effects affecting the determination of flows from local helioseismic analysis of regions over different parts of the observable disk, not all well understood. In this study we characterize those systematic effects with higher spatial resolution, so that they may more effectively be accounted for in mapping temporal and spatial evolution of the flows. Leaving open the question of the mean structure of the global meridional circulation and the differential rotation, we describe the near-surface flow anomalies in time and latitude corresponding to the torsional oscillation pattern in differential rotation and analogous patterns in the meridional cell structure as observed by SDO/HMI.

1. Introduction

The mean properties of solar rotation, zonal flows and meridional circulation close to the surface have been well studied. The Sun rotates substantially faster at the equator than

at the poles. Over and above the mean differential rotation profile there are bands of mean zonal flows corresponding to slight prograde and retrograde variations in the local rotation rate at different latitudes that change with the solar cycle. There is also a regular weak flow of material from the solar equator to the poles. The most reliable measurements of these dynamical features are for the low- and mid-latitude regions. Limitations of observation and analysis techniques have resulted in rather uncertain results at high solar latitudes. There are also uncertainties in the details of the longitudinal variation of solar dynamics. Observations made by the Helioseismic and Magnetic Imager (HMI) on board the Solar Dynamics Observatory (SDO) allow us to examine both of these issues. In this paper we use these data to study the evolution of spatially resolved features in the zonal and meridional flows at high solar latitudes.

The presence of zonal flows was first deduced from surface Doppler measurements. A long-period oscillation, dubbed the "torsional oscillation," was identified by Howard & Labonte (1980). It consists of alternating latitude bands of slightly faster and slower rotation migrating equatorward as the solar activity cycle progresses. These were confirmed by Ulrich (1998, 2001). Poleward meridional circulation was detected at the surface using direct Doppler measurements (Labonte & Howard 1982; Hathaway et al. 1996).

Both zonal and meridional flows seen at the surface have been confirmed by various helioseismic studies. The longitudinally averaged, north-south symmetric part of the zonal flows has been seen by inverting global modes of solar oscillations (e.g. (e.g. Kosovichev & Schou 1997; Antia & Basu 2000; Howe et al. 2000; Antia & Basu 2013; Howe et al. 2013). The lack of sensitivity of the global data to features at very high latitudes means that these investigations could not probe the polar regions properly. Additionally, global helioseismic inversions do not give any longitudinal resolution, nor can they readily separate the contributions from the northern and southern hemispheres. Local helioseismic techniques, however, can address these problems.

Among the more widely used local helioseismic techniques, ring-diagram analysis (Patrón et al. 1997; Hill 1988) uses three-dimensional power spectra of small regions of the Sun to measure the mean horizontal motions over those regions, allowing us to study localized solar dynamic phenomena. The analysis technique has allowed us to study hemispherical differences in the near-surface rotation rate (e.g. Basu et al. 1999; Haber et al. 2000), as well as meridional flows (e.g. Basu et al. 1999; Haber et al. 2002; Basu & Antia 2010).

Determining the exact nature of the meridional flows at high latitudes has proved to be a challenge. At low and middle latitudes, the flow of material is poleward in both hemispheres. The situation at high latitudes is less clear — even the sense of the flow is difficult to determine. Equatorward cells at very high latitudes have been reported, but it has

been shown that these may be due, at least in part, to systematic errors in the measurements at large distances from disk center (Zaatri et al. 2006; Zhao et al. 2012).

The high-resolution, high-cadence, nearly continuous data available for the current solar cycle from the HMI instrument make it possible to study spatially resolved flows up to very high latitudes. Surface Doppler data were used by Hathaway et al. (2013) to study the motion of supergranules; they found long-lived anomalies of slower-than-average (retrograde) zonal flows, which they interpreted as the signatures of giant cell convection. Using the HMI Doppler data for local helioseismic analysis of solar near-surface dynamics, we can see similar long-lived features close to the poles. We use data collected over a four-year period from 2010 to 2014 that covers the rising phase of cycle 24. We use the ring-diagram technique, and unlike prior investigations such as those of Komm et al. (2014) and 2015, we use tiles as small as $5^\circ \times 5^\circ$ instead of the usual $15^\circ \times 15^\circ$ to achieve better spatial resolution.

In Section 2 we discuss the data analysis. Detailed results are presented in Section 3, and we conclude with a summary of the results in Section 4.

2. Data Analysis

The Helioseismic and Magnetic Imager (HMI) has been producing a nearly uninterrupted series of full-disk solar photospheric Dopplergrams suitable for high-resolution local helioseismic analysis at a cadence of one every 45 sec for over 4.5 years. One of its fundamental mission science products is a collection of "ring-diagram" analysis products — power spectra, ring (ridge) fit parameters, and depth inversions of certain of the horizontal flow parameters (Bogart et al. 2011a,b). The ring analyses are performed on three different scales, for sets of overlapping regions of approximate diameters 5°, 15°, and 30° heliographic, or about 60, 180, and 360 Mm respectively. Most published work has focused on the data for the 15° regions, in part because this scale is also accessible to the lower-resolution data from the Michelson Doppler Imager (MDI) on the earlier SoHO mission and the ongoing GONG project (see Baldner et al. 2013, and references therein). Furthermore, most of the studies of the evolution of synoptic flow structures have been limited to data from regions on the central meridian. As we show here, the quality of the mode fits is nearly uniform over most of the solar disk, suggesting that mode fits from off the meridian may contribute substantially to the quality of the measurements, particularly over short time samples.

The data for the 5° regions do not yield mode sets rich enough to support well-resolved depth inversions, as they are normally sensitive to only the f-mode and two or three orders of the p-modes, penetrating to depths of about 1% (7 Mm) of the solar radius (see Figure

1). They do however provide spatial resolution adequate to map structures potentially associated with the zonal belts and regions of magnetic activity. They also provide fine enough spatial resolution to address questions about systematic disk-position effects which may bias measurements of the structure of the large-scale mean flows (e.g. Zhao et al. 2012). These systematic effects are of particular concern for measurement of the meridional circulation at high latitudes, an important parameter for models of solar cycle evolution. As we show here, these effects do not have a simple radial nor east-west dependence. Nevertheless, they appear to be quite stable over time. This suggests that they have little or no effect on the short-term evolution of the flow patterns, which are the focus of this study.

In the HMI ring-diagram analysis pipeline, sequences of Dopplergrams are mapped into sets of tiles of equal size and shape, with each tile fixed at particular Carrington coordinates (*i.e.* tracked at the Carrington rotation rate). Three different tile sizes are mapped, the tiles being tracked for approximately the time during which they would rotate through their width. The smallest tiles are mapped at the equivalent full resolution of HMI at disk center, $0^\circ.04$ heliographic per pixel, with widths of $5^\circ.12$, and tracked for 576 min (768 HMI 45-sec Dopplergams). The tile centers are spaced at intervals of $2^\circ.5$ in latitude and multiples of $2^\circ.5$ in longitude, so that they are roughly equally spaced on the surface, and extend to about 80° from disk center. There are either 2727 or 2748 such tiles at each analysis time, depending on B_0, the heliographic latitude of Earth. The analyses are repeated at intervals of 5° in synodic rotation, 72 per Carrington rotation. Apart from occasional interruptions in the data stream caused by eclipses, instrument calibrations, spacecraft maneuvers, and accidents, there are between 196,344 and 197,856 ring-diagram spectra analyzed per rotation.

Two procedures are used to fit the power spectrum to obtain the mode parameters. A fast algorithm designed to estimate just the frequency displacements necessary for determinations of the mean horizontal flow is applied to each region; its fit parameters are inverted to obtain the published flows for the larger regions. For the 5° regions, however, the number of modes fit is too small for useful inversions. Better fits are obtained using the model described by Basu et al. (2004):

$$P(k_x, k_y, \nu) = \frac{e^{B_1}}{k^3} + \frac{e^{B_2}}{k^4} + \frac{\exp(A_0 + (k - k_0)A_1 + A_2(\frac{k_x}{k})^2 + A_3\frac{k_x k_y}{k^2})S_x}{x^2 + 1} \quad (1)$$

where

$$x = \frac{\nu - ck^p - U_x k_x - U_y k_y}{w_0 + w_1(k - k_0)}, \quad (2)$$

$$S_x = S^2 + (1 + Sx)^2, \quad (3)$$

The 13 parameters A_0, A_1, A_2, A_3, c, p, U_x, U_y, w_0, w_1, S, B_1, and B_2 are determined by independently fitting each ridge in the spectrum. The parameters of most interest are U_x and U_y, representing the mean advection in the zonal and meridional directions in the local plane geometry at the center of the region.

These fits are too time consuming to perform over all of the larger regions, but they can be and are applied to all of the 5° regions. Because they provide robust estimates of all of the mode parameters over almost the entire disk with minimal cross-talk and fairly uniform precision, they are the ones we have chosen to use for this study. The number of ridges that can be fit is still of course limited by the small size of the regions; typically only the f-mode and the first 3 p-mode ridges yield substantial numbers of modes (Figure 1). However, the fitting is of nearly uniform quality over the disk, the number of modes fit among the lowest 4 orders being approximately constant from disk center to about $\mu = 0.3$ (72°.5), as shown in Figure 2. For estimation of azimuthal averages of the flows, use of the fits from off of the central meridian increases the available data by a factor of 42.

Note that there is a systematic change in the U_i parameter values between the fits for Carrington Rotations 2125 and 2126 (*i.e.* beginning 2012 July 18). Analysis of data from the transit of Venus on 2012 June 5–6 revealed that the original estimate for the HMI position angle with respect to the Carrington rotation axis was slightly in error. An adjustment of 0°.070206 to the position angle in processing of the Doppler and other data was made beginning 2012 August 31 (actually at 23:48 on August 30) and the records for all data prior to that time subsequently adjusted to reflect the correction. Data through the end of CR 2125 had however already been processed using the old values of the position angle for the mapping and tracking. There is thus a spurious meridional component of the solar rotation, plainly visible in comparing results from before and after the change (see Figure 7; also Figure 12), biasing the measured meridional flows by about 2.5 m-s^{-1} in the earlier data.

In order to examine temporal variations in the "mean" flow patterns, we have divided the data into eight overlapping sets as close to one year in length as possible (Table 1), in order to remove systematic biases due to the annual variation of the observer latitude of ±7°.25. Because of the aforementioned adjustment in the assumed image position angles, averages for Years 2.5 and 3 will include data with both values and consequently mixed leakages of rotation into the mean meridional flow.

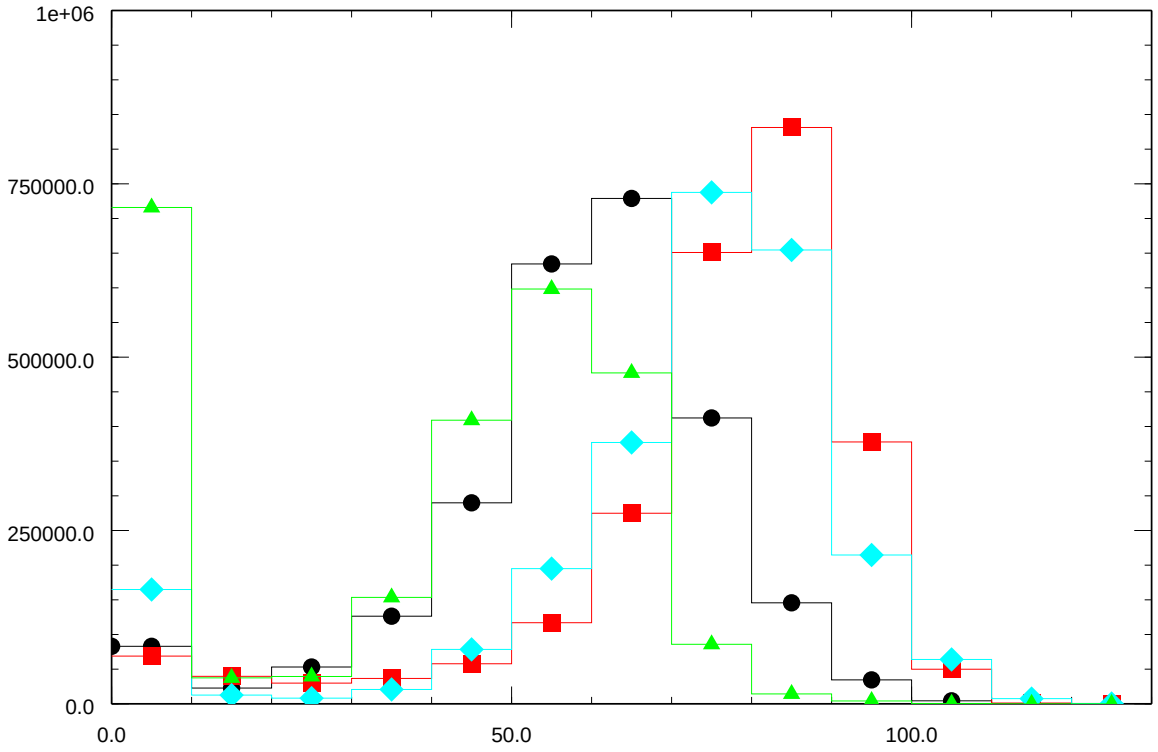

Fig. 1.— Histogram of the total number of regions with the given number of mode fits, by radial order n, during a period of about one year (CR 2143–2155, 2013 October 25 – 2014 October 14). Symbol codes: $n = 0$ black circles, $n = 1$ red squares, $n = 2$ cyan lozenges, $n = 3$ green triangles.

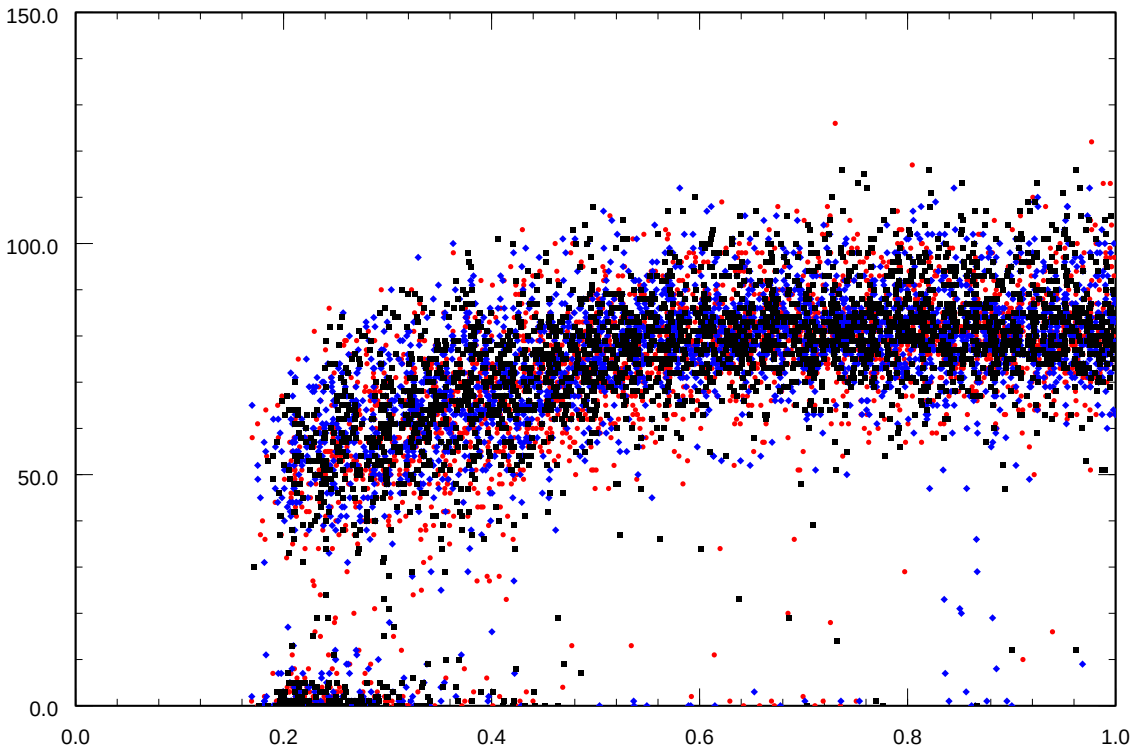

Fig. 2.— Scatter plot of the number of fits of order $n = 2$ modes over the entire disc as a function of the mean central angle of the center of the region $\mu = \cos(\theta)$ as it is tracked during three sample time intervals: 2121:340 (2012 March 06, when $B_0 = -7^\circ.25$, red circles), 2154:115 (2014 September09, when $B_0 = +7^\circ.25$, blue lozenges), and 2144:160 (2013 December 06, when $B_0 = 0^\circ$, black squares).

Year	Start CR:CL	Start Time (UT)	End CR:CL	End Time (UT)
1	2096:250	2010 May 01 02:12	2109:115	2011 Apr 30 21:34
1.5	2102:010	2010 Oct 29 15:58	2116:235	2011 Oct 29 11:18
2	2109:110	2011 May 01 06:39	2123:335	2012 Apr 30 02:01
2.5	2116:230	2011 Oct 29 20:24	2129:095	2012 Oct 28 15:45
3	2123:330	2012 Apr 30 11:06	2136:190	2013 Apr 30 15:32
3.5	2129:090	2012 Oct 29 00:51	2143:310	2013 Oct 29 05:17
4	2136:185	2013 May 01 00:37	2149:050	2014 Apr 30 19:59
4.5	2143:305	2013 Oct 29 14:23	2156:170	2014 Oct 29 09:43

3. Results

When we examine the mean values of the U_i parameters at each latitude and (Stonyhurst) longitude averaged over exactly four years we see that (a) there are systematic and significant east-west variations in both the zonal and meridional flows at a given latitude; and (b) there is evidence for a consistent meridional flow reversal poleward of about $\pm 60^\circ$ (Figures 3 & 4). It is somewhat difficult to compare the systematic disc variations in the zonal velocity that we see with those from the similar lower spatial resolution analyses reported by Komm et al. (2015) because they compare the systematic anomalies with respect to a differential rotation model; but in any case the main variations that we see occur at center-to-limb distances beyond the range of their data. The azimuthal variations in the mean meridional flow that we see exhibit a similar structure in the northern hemisphere to those that they see at the times when the solar north pole is tipped towards the Earth; but the systematic disc variations that we see are of much lower amplitude. Again, the latitudes where our data show consistent evidence for a high-latitude reversal are at and beyond the limit of theirs.

There are also small but significant year-to-year variations in the meridional flow profile around the latitudes of activity. The large zonally symmetric component to the zonal flow parameter merely reflects the fact that the analysis regions are tracked at a uniform rate to account for the rotation of the coordinate system, and consequently exhibits the near-surface differential rotation in the outer 1% of the Sun, the average sampled depth. East-west variations must certainly be spurious artifacts of either the observational or analysis procedures, possibly related to center-to-limb variations or the symmetry breaking associated with tracking the analysis regions to compensate for the rotation of the coordinate system. The former at least calls into question the reality of the observed high-latitude counter cell in the meridional flow. The arguments advanced by Zhao *et al.* (2012) for rejecting a

comparable result in time-distance analysis do not however apply in this case, as significant limb effects in the mean zonal flow parameter do not show up until about longitude 75° (Figure 5). We also see small but significant hemispheric asymmetries in the mean zonal flow (rotational) profile at the level of a few m-s^{-1} at all latitudes between about 10°and 75°, with faster motion in the southern hemisphere, particularly around latitude −50° (Figure 6).

Apart from the systematic shift in the meridional flow parameters globally due to the correction of the position angle, the structure of the mean flow parameters at each location on the disk remain very stable throughout the course of the mission (Figure 7). Certain features, such as the apparent variation from east to west of the flow parameters, can scarcely be real, and must result from systematic effects in the interpretation of the measurements. Others, such as the reversal in sign of the meridional flow parameter near the poles, suggestive of a high-latitude counter cell, may be real. Both of these features, east-west asymmetries, and a meridional sign reversal at high latitudes, appear broadly in the fast fits as well as the 13-parameter ring fits, though with slightly different structure and amplitude. The fact that there is an east-west variation in the year-to-year changes in the zonal flow as well as in the mean values indicates that there is a sensitivity effect. The apparent enhancement in the zonal flow at the east limb is certainly consistent with a spurious measured "flow" inwards from limb to disk center, such as has been posited by Zhao et al. (2012) for the time-distance measurements and demonstrated to be an expected effect (Baldner & Schou 2012). It could explain the observed meridional flow reversal at the poles, with a comparable magnitude of order 10 m-s^{-1}. It is not however balanced by a comparable reduction in zonal flow at the west limb. Whether the high-latitude meridional flow parameter reversal does in fact reflect a more-or-less permanent feature of the meridional circulation near the poles cannot yet be established without a better understanding of the spatial systematics in the analysis of the measurements.

The year-to-year variations in annual averages of the zonal flow at different latitudes and Stonyhurst longitudes show significant variations at the 2–5 m-s^{-1}-yr^{-1} level, consistent with the amplitude of the global torsional oscillation signal which is azimuthally averaged and (at least for helioseismic measurements) symmetrized about the equator (Howe et al. 2013). Note that both the zonal rotational acceleration and deceleration rates were substantially larger in the last year than the first, with a marked hemispheric asymmetry in both the amplitude and the zonal extent of the decelerated belts, and a bifurcation of the equatorial accelerated zone into two, centered slightly to the south of the equator.

Variations in the mean meridional flow are more marginal. In the northern hemisphere there has been a consistent strengthening in the poleward flow of about 3 m-s^{-1}-yr^{-1} in a

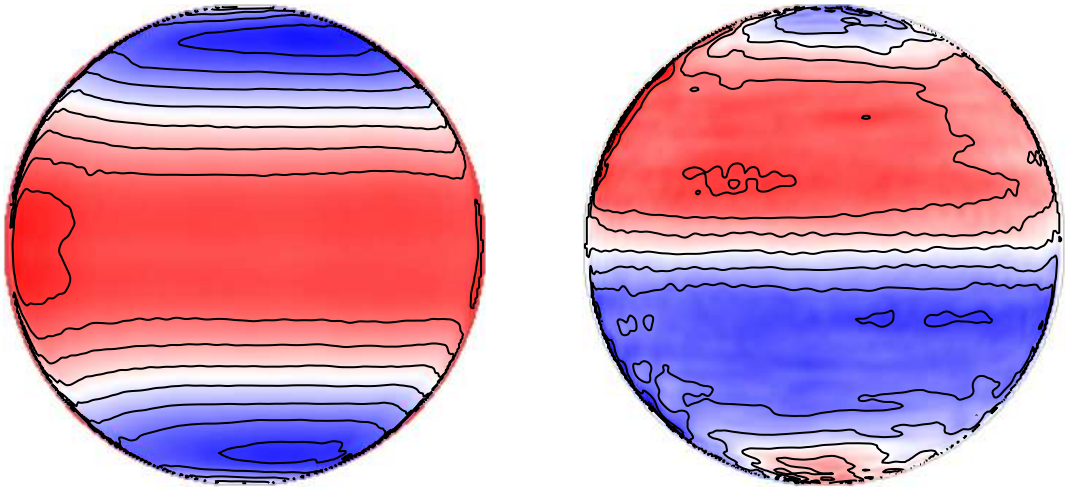

Fig. 3.— Mean values of U_x (left) and U_y (right) over the 4-year interval 2096:250–2149:050 (2010 May 1 to 2014 May 1) integrated over all modes in the range $n = 1$–3 with R_t between 0.9875 and 0.9975, as functions of heliographic latitude and Stonyhurst longitude. The color scales range from -200 – +25 m-s^{-1} with 25 m-s^{-1} contours for U_x, and between ±20 m-s^{-1} with 5 m-s^{-1} contours for U_y.

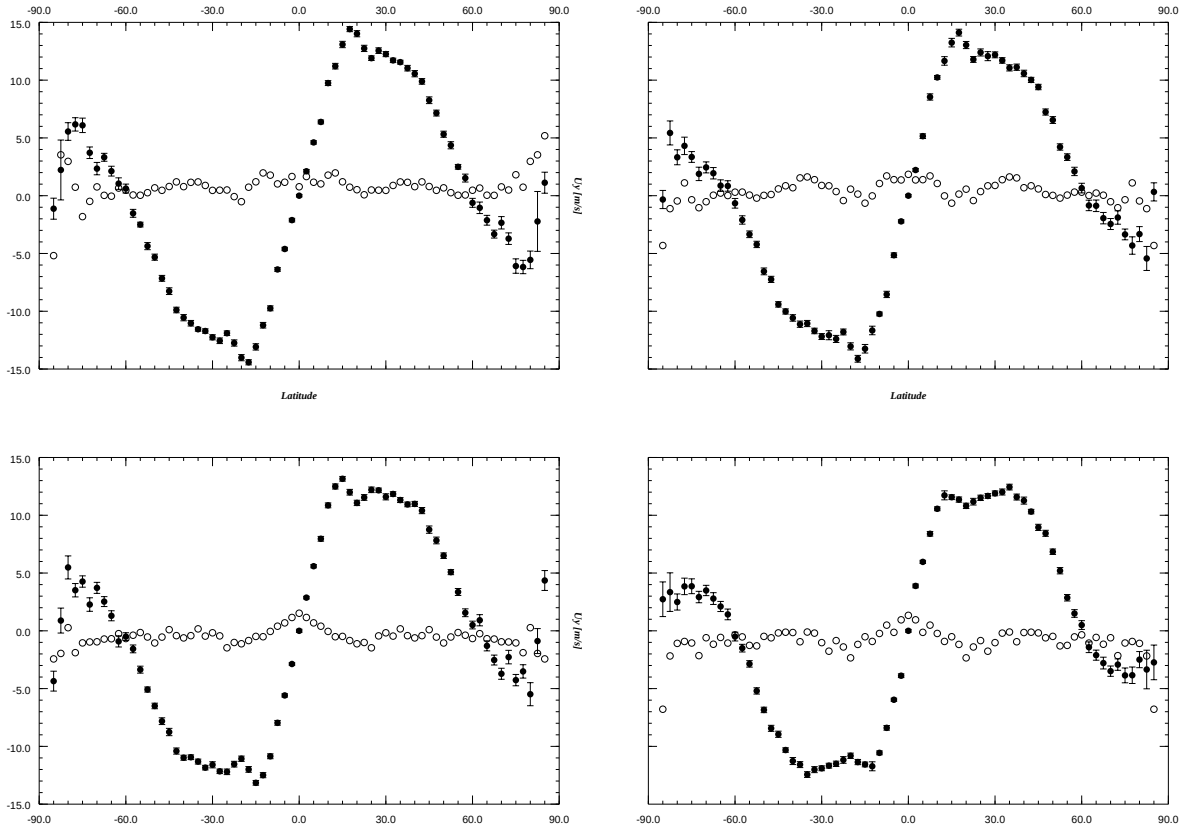

Fig. 4.— Zonally symmetric (open symbols) and anti-symmetric (filled symbols) components of the meridional flow parameter U_y averaged over all longitudes for the same mode sets as in Fig. 3 for Years 1 (upper left), 2 (upper right), 3 (lower left), and 4 (lower right). Standard error bars are shown for the anti-symmetric component only; those for the symmetric components at the same latitude are of course the same.

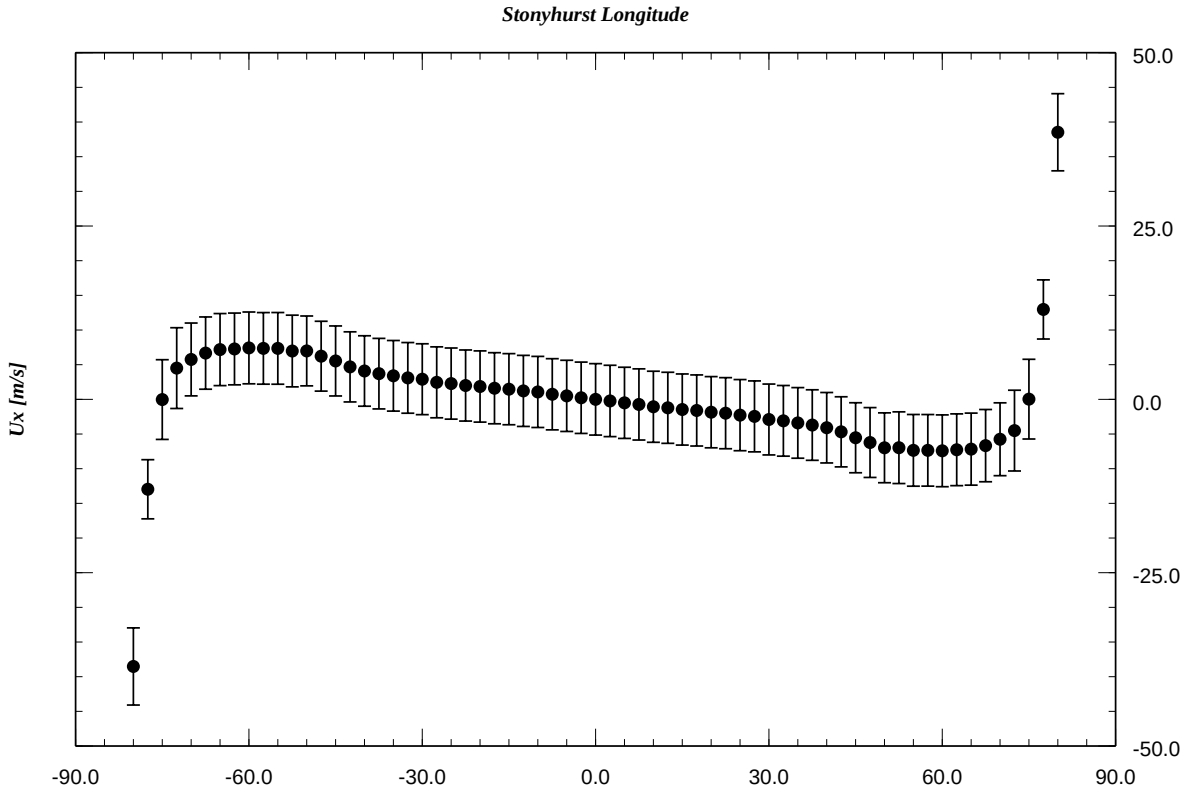

Fig. 5.— Longitudinally antisymmetric component of the 4-year averaged values of the zonal flow parameter U_x averaged over all latitudes for the same mode sets as in Fig. 3, shown as a funtion of Stonyhurst longitude.

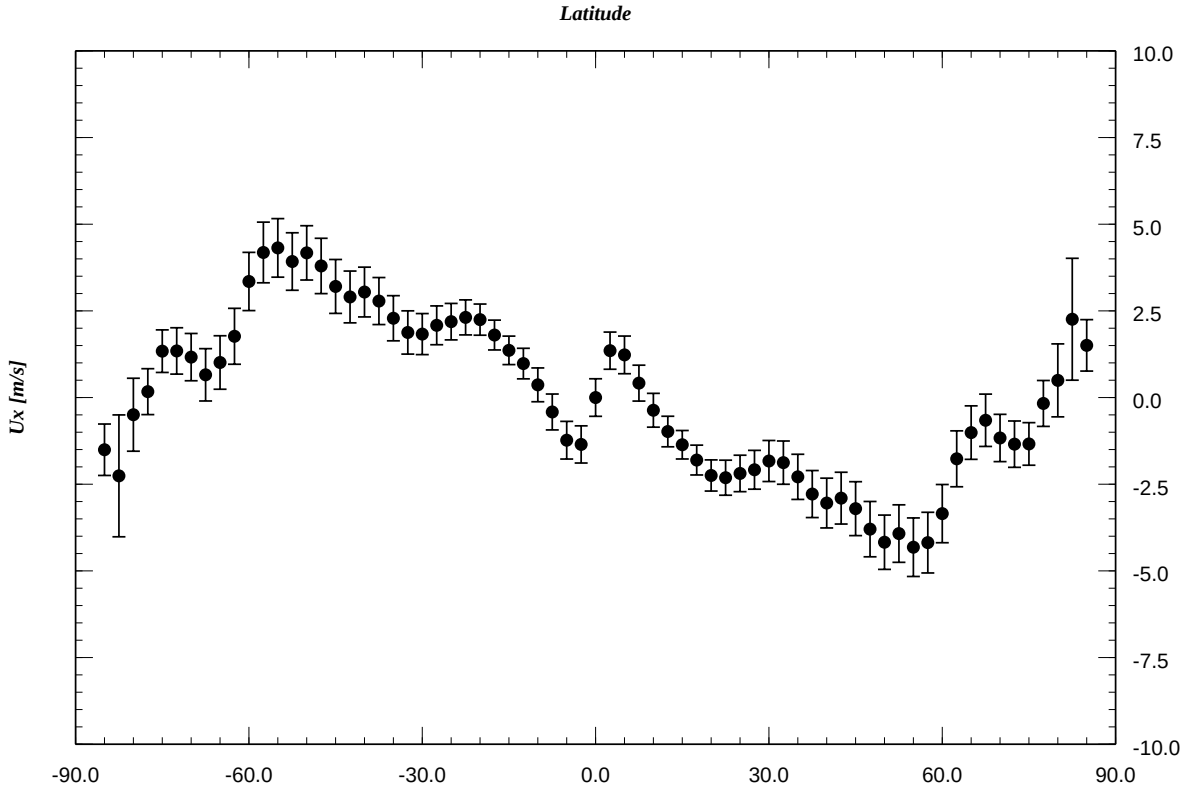

Fig. 6.— Zonally antisymmetric component of the 4-year averaged values of the zonal flow parameter U_x averaged over all longitudes within $\pm 70^\circ$ for the same mode sets as in Fig. 3.

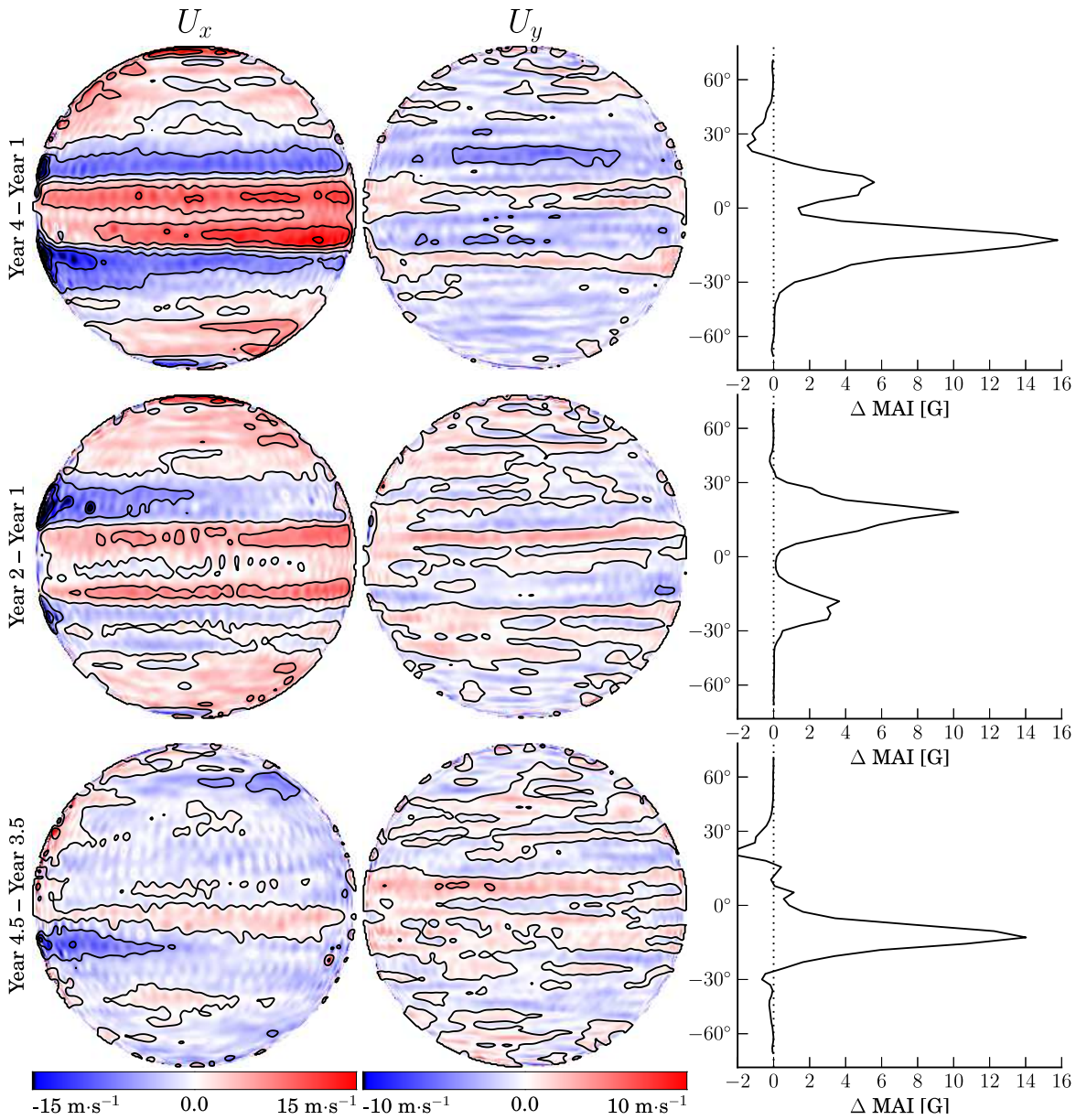

Fig. 7.— Changes in the 1-year means of U_x and U_y between Year 1 and Year 4 (top), Year 1 and Year 2 (middle), and Years 3.5 and 4.5 (bottom). The color scales range between ±15 m-s^{-}1 for U_x and ±10 m-s^{-1} for U_y with 5 m-s^{-1} contours in both. For the year-to-year changes we also show the changes at each latitude of the mean values of the Magnetic Activity Index (MAI), defined as the average within each tracking cube of the absolute value of all HMI line-of-sight magnetic field values (from data series *hmi.V_45s*) in excess of 50 G.

narrow zone around latitude 7°.5 and a corresponding weakening of about -1.5 m-s^{-1}-yr^{-1} in a somewhat broader zone around latitude 15°–20°. Trends in the southern hemisphere are more confused. Strengthening of the poleward flow centered around latitude -12°.5 in the first year has migrated to around -30° in the last, while the zones of weakening have correspondingly migrated toward the equator. (As discussed above, the measured overall southward flow increase from the first year to the last is only an artifact of the change in the assumed position angle used in the tracking.)

Turning our attention to variations in the flow patterns that can be localized in space and time, we note two striking features (Figures 8 & 9). There are anomalies in the zonal flow at high latitudes that manifest themselves along distinct bands in the Carrington coordinate system of width about 10°. They stretch from southwest to northeast in the northern hemisphere and oppositely in the southern hemisphere, consistent with dragging of a feature by the differential rotation shear. They can be clearly seen in Figure 10, which combines the standard synoptic maps with polar views for two selected rotations. These features persist for several rotations, with a gradual increase in their inclination angle, again consistent with shear dragging. Both this winding and overall eastward propagation consistent with surface differential rotation are more vividly illustrated in Figure 11. Apart from these extended high-latitude features, there are localized flow anomalies, equally visible in the meridional and zonal directions, at lower latitudes that are clearly associated with active regions, a well-established phenomenon; the anomalies in CR 2109 can be readily identified with AR 11190, 11193, 11195, 11199, 11203, and 11204, while those in CR 2136 are associated with AR 11731 and 11734–11736.

The torsional oscillation in zonal flow anomalies at different latitudes is fundamentally a function of two dimensions, time and latitude, as it is based on azimuthal averages of the signal at each latitude over the course of a rotation (or sometimes longer, as with the GONG, MDI, and HMI helioseismic measurements based on 36- and 72-day averages — cf. Howe et al. 2013). Helioseismic measurements based on global mode inversions also provide only the symmetric component of the torsional oscillation signal over the northern and southern hemispheres. Combining the present results which are spatially resolved in two dimensions from the whole time range observed allows us to produce a plot equivalent to standard plots of the torsional oscillation, but with longitudinal resolution within each rotation and the hemispheres separately resolved (Figure 12).

The localized small meridional flow anomalies, by contrast, exhibit only occasional high-latitude structures, and they seldom last for more than a single rotation. The anomalies are dominated by the localized flows away from active regions. The equivalent plot to standard torsional oscillation ones (Figure 12) exhibits alternating bands of northward and southward

flow anomalies at all latitudes, with a period of one year. These are almost certainly due to an error in the Carrington elements. Note especially that the amplitude of this annual variation decreased (but did not completely disappear) at the time the value of the HMI camera position angle with respect to the nominal Carrington axis was corrected.

Although the fitted mode sets from such small regions are too limited for decent inversions of the depth structure of these features, we can get rough estimates of their depths by simply dividing the mode sets into groups with different values for the classical turning point ν/ℓ. Figure 13 compares the values along cuts at selected latitudes from contiguous synoptic maps of the anomalous zonal flows for three rotations, but constructed for two different sets of modes, one with turning points at a depth of about 4 ± 1 Mm and the other at about 6 ± 1 Mm. It is evident that these anomalous zonal flow bands extend to depths of at least 1% of the radius. At the lower latitude there is no significant difference between the anomalous flows at the two depths, both showing the same longitudinal pattern. At the higher latitudes the anomalies clearly have greater amplitude at the greater depth, although they are still highly correlated, the peaks and valleys occurring at the same longitudes; in all cases the probability of exceeding the correlations in random distributions with the same statistics are far less than 10^{-3}. The greater amplitude of the negative anomaly at the greater depth actually runs counter to the general trend expected in the radial differential profile at high latitudes, but in any case it is clear that its amplitude remains larger than any azimuthally independent differences due to radial differential rotation.

4. Conclusions

Ring-diagram analysis of high-resolution Doppler data from HMI can resolve features in the near-surface flow fields with limited depth resolution at size scales down to about 50 Mm and extending almost to the poles. There is some evidence for a regular counter-cell near the photosphere at very high latitudes in the mean global meridional circulation, but absolute determinations of mean flows at high latitudes are compromised by systematic effects on both the measurements and analysis at large center-to-limb angles that are not yet fully understood.

Despite the uncertainties in determining mean flows globally, it is evident from several years' data that the systematic center-to-limb effects are stable. By removing the measured means for observations at each disc position, and carefully averaging over entire years so that all values of the heliographic observer latitude are equally sampled, we can determine residuals in the zonal and meridional velocities with a spatial resolution down to that of the ring analysis itself, and a temporal resolution of less than or order of a single Carrington

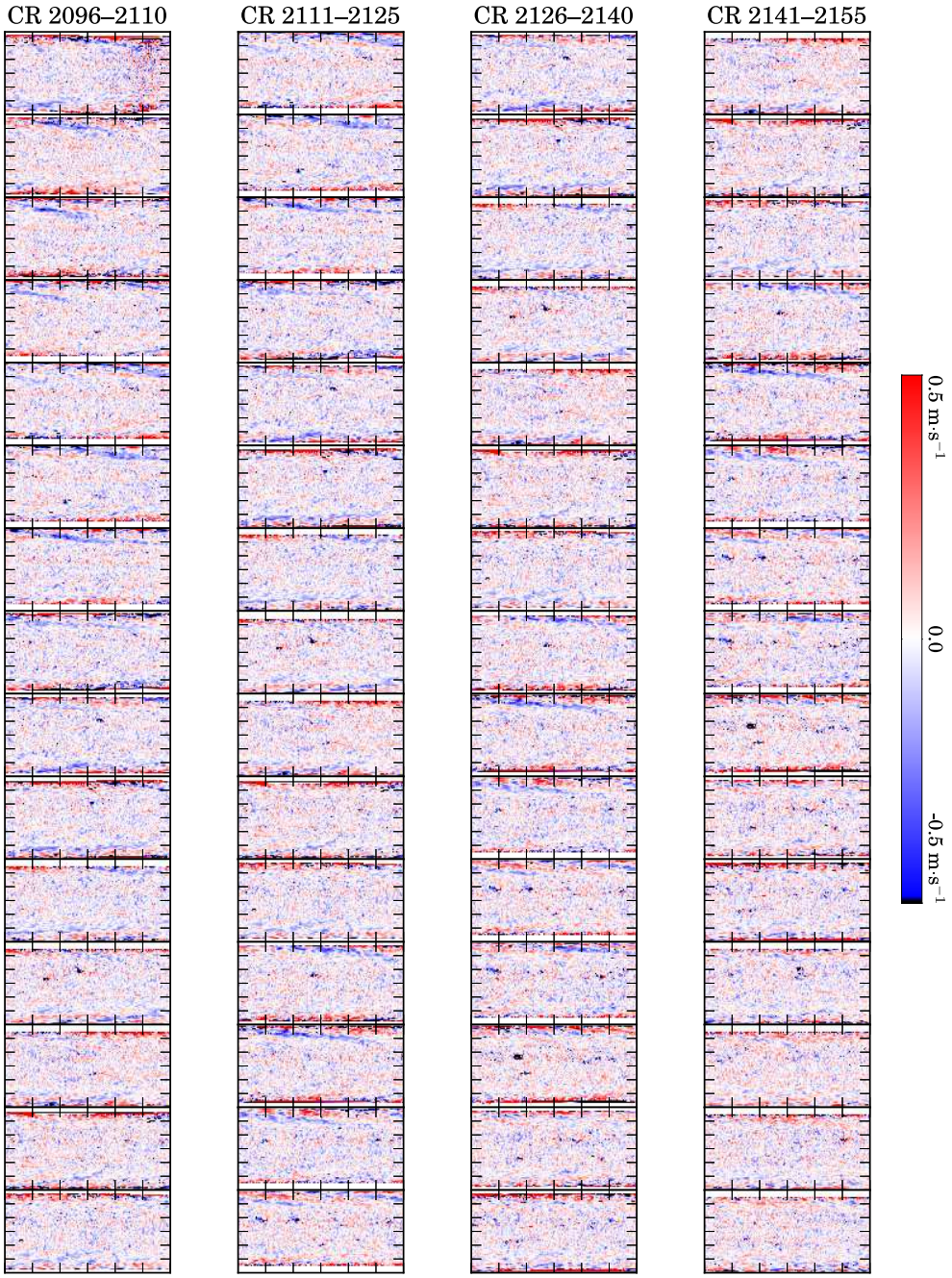

Fig. 8.— Synoptic maps for each Carrington rotation of the U_x flow anomalies, defined as the differences between the values at each heliographic location and the mean values at the corresponding Stonyhurst locations over Years 1–4, averaged over all observations during the rotation, for the same range of modes. The color scale ranges between ± 0.5 m-s^{-1}, with red representing a positive (super-rotational) anomaly.

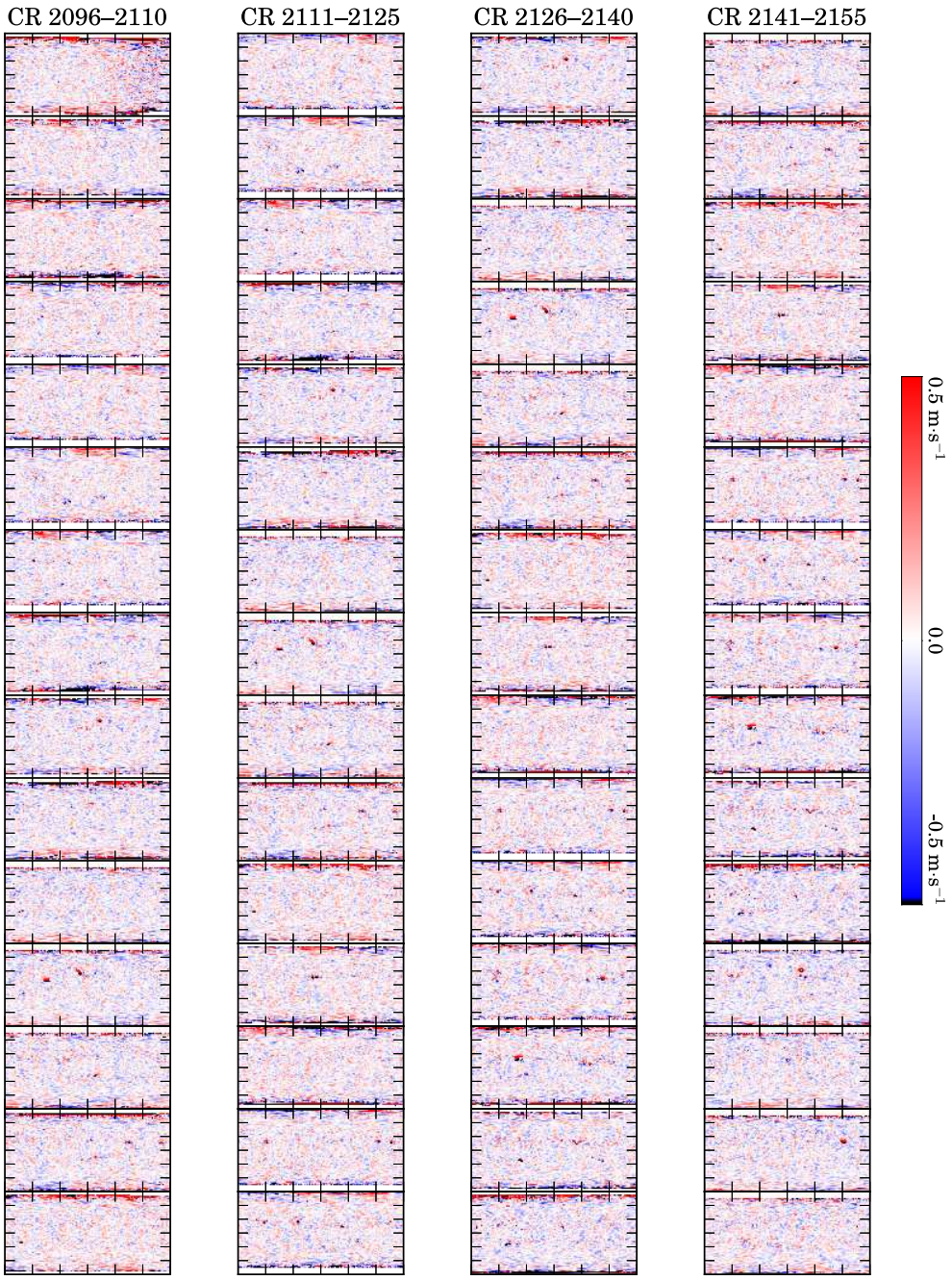

Fig. 9.— Same as Figure 8, for the U_y flow anomalies. The color scale ranges between ±0.5 m-s^{-1}, with red representing a positive (northward) anomaly.

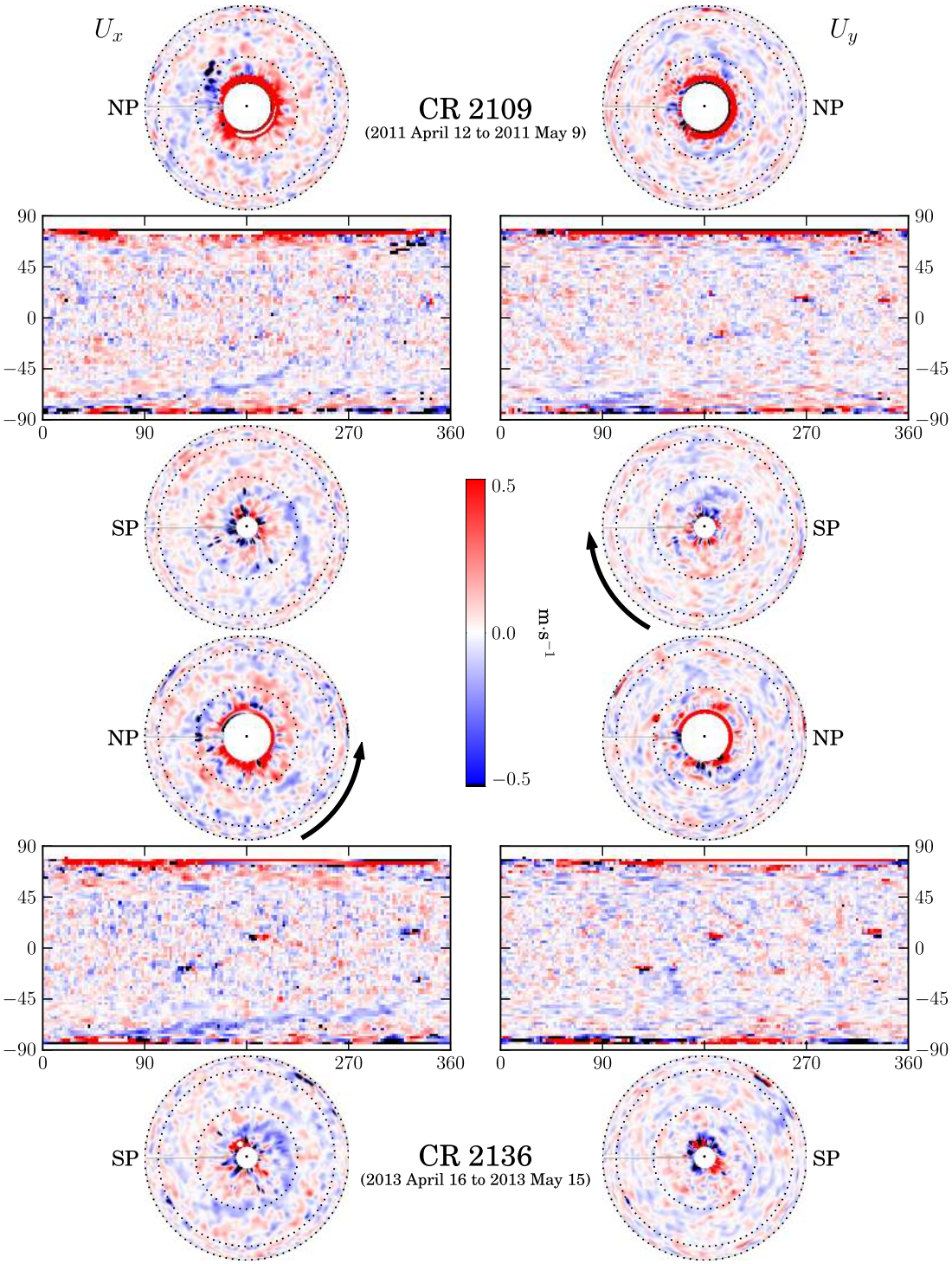

Fig. 10.— Synoptic maps of the zonal flow anomalies U_x (left) and U_y (right) for two selected Carrington rotations two years apart, showing orthographic projections from above the north and south poles above and below the standard plate carrée projections. The two rotations are at times when the south pole is tipped slightly toward the Earth, accounting for the more extended coverage at high southern latitudes. Carrington longitude 0° is at left in both polar plots, with longitude increasing in the direction of solar rotation as shown by the arrows.

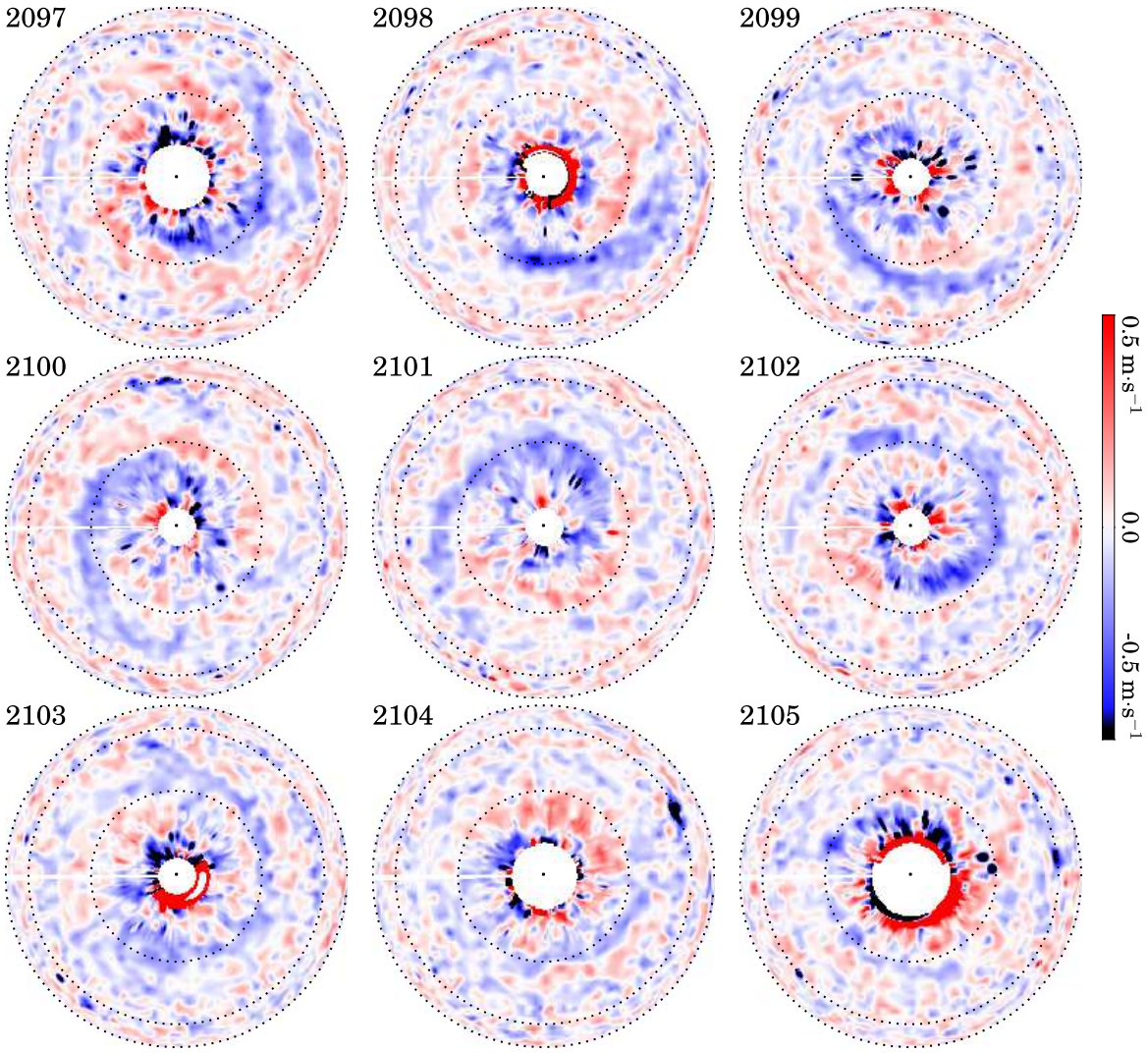

Fig. 11.— Synoptic maps of the zonal flow anomalies in the northern hemisphere for nine successive Carrington rotations, plotted in an orthographic projection centered on the north pole. Carrington longitude 0° is at left, with longitude increasing counter-clockwise, the direction of solar rotation. The mean sampling times of course increase clockwise, so the data from just below the 0° half-line are sampled one rotation later than the data just above. The color scale is the same as in Fig. 8. The dashed circles are latitude lines at intervals of 30°˙ The varying size of the unsampled region around the pole is due to the tipping of the pole toward and away from the Earth-orbiting observatory over the course of the year.

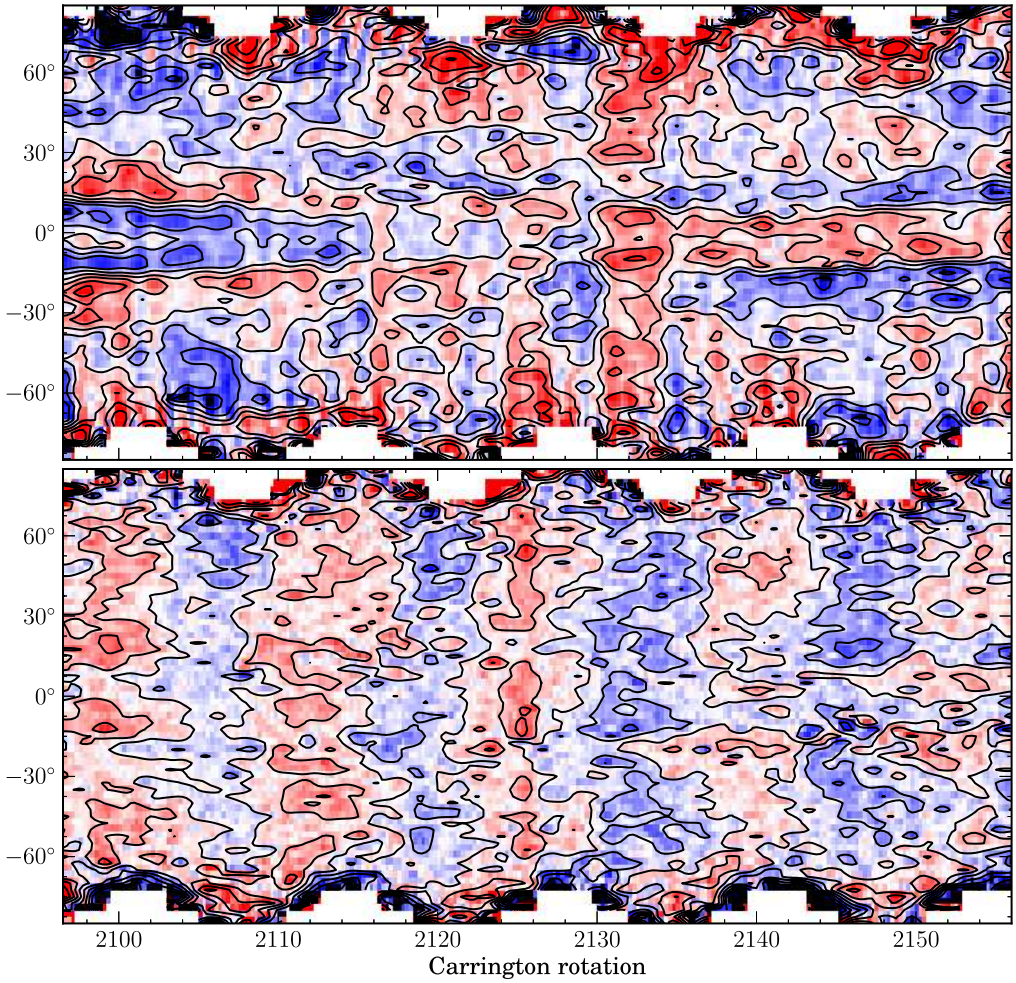

Fig. 12.— Anomalies for the zonal (top) and meridional flow components relative to the 4-year means measured at the same disc positions, averaged over all longitudes and over a full Carrington rotation and sampled four times per rotation, plotted as functions of time on the horizontal axis and latitude on the vertical. The color scale range is ± 10 m-s^{-1} for both, with contours at 2.5 m-s^{-1} intervals. The time range covered extends from CR 2096.5 (1996 May 6) to 2056.0 (2014 October 14)

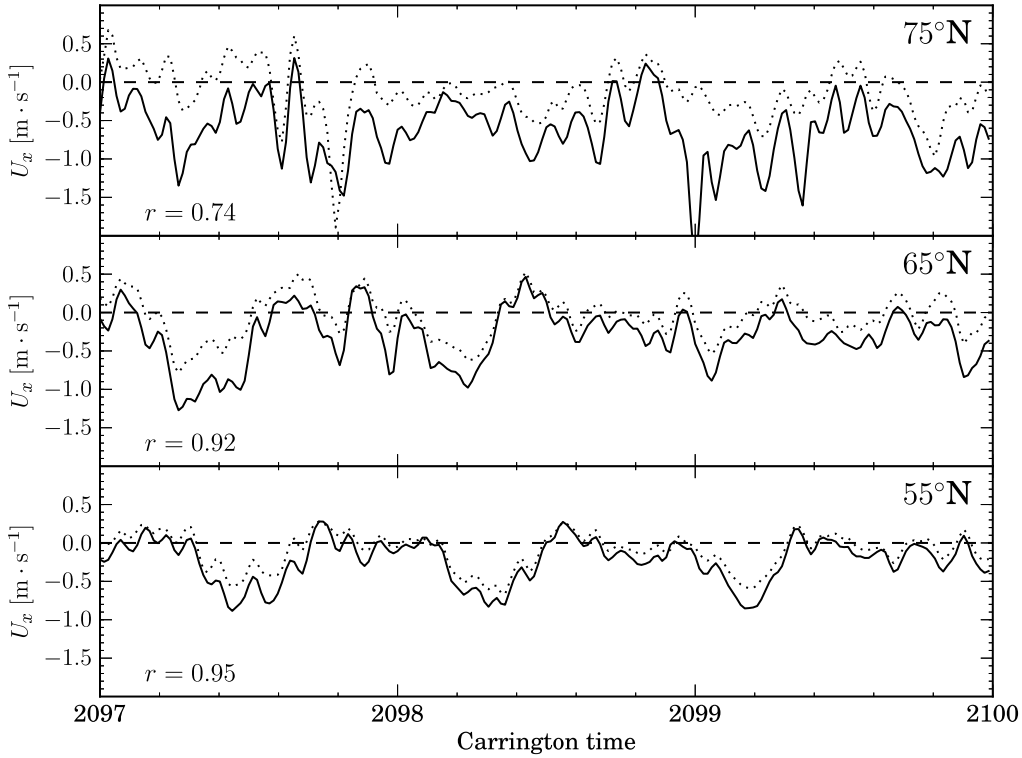

Fig. 13.— Comparison of the zonal flow anomalies during CR 2097–2099 at selected latitudes for two different mode sets. The solid curve displays the local anomalies determined from modes restricted to those with classical turning points between 0.9900–0.9925 (depth 5.25–7 Mm), the dotted curve to those in the range 0.9925–0.9950 (depth 3.5–5.25 Mm). Each set of curves represents the mean zonal flow anomalies as a function of longitude within a latitude strip of width 10° centered on the labeled latitude. They are equivalent to plots of the values along horizontal cuts at different latitudes in a series of three consecutive synoptic plots of Figure 8. r is the correlation coefficient between the flow anomalies at the different depths

rotation. We find that there are belts of localized anomalies in the zonal flow at high latitudes persisting for five or more rotations. These belts are elongated in longitude, at least qualitatively consistent with the shear expected from differential rotation of a feature initially aligned along a meridian.

It is interesting to speculate on the nature of the persistent structures seen in the spatial distribution of the flow anomalies, particularly those of the zonal flow at high latitudes. It is tempting to interpret these flow anomalies as the eastward or westward motions at the surface of extended "banana cells" convective structures, as suggested by Hathaway et al. (2013), that have been "wound up" by differential rotation. Certainly the drift of the spiral pattern in the direction opposite to that of the rotation of the Carrington frame, especially evident in Figure 11, is to be expected from the slower rate of surface rotation at high latitudes. On the other hand, there is little evidence of tightening of the spirals from one rotation to the next. Quantitative investigation of the motions of these patterns in comparison with the known depth structure of the differential rotation profile might yield information on the depth at which they are seated, and whether they are indeed surface manifestations of deep convective cells. A point to note is that although nearby zonal flow anomalies of opposite sense would imply divergence or convergence at lower latitudes, near the poles they represent instead a zonal shear between the inner and outer arms of the spiral. This might be related to the development of the torsional oscillation at high latitudes, with its implications for evolution of the solar cycle.

Although the meridional flow anomalies do not exhibit nearly as marked nor persistent structures at high latitudes, there appears to be a general tenedency at lower latitudes for them to organize themseleves in about eight to twelve alternating bands of northward and southward motions. Whether this pattern is statistically significant remains to be established; if it is, it would suggest a large-scale sectoral structure of cyclonic and anti-cyclonic flows that should be related to the zonal flow anomalies at the higher latitudes. One notable feature in the high-latitude patterns of the meridional flows is that rather then being organized into spiral structures, the tend to exhibit simply a single-celled azimuthal asymmetry. This is what would be expected if there were a cross-polar flow. If such flows were slightly displaced from the exact pole, their azimuthal averages might account for the apparent counter cell in the mean meridional flow that we observe at high latitudes.

We are grateful to David Hathaway and to an anonymous reviewer for helpful comments and suggestions. This research was supported in part by NASA Contract NAS5-02139 and in part by NASA Grant NNX14AH08G, both to Stanford University.

REFERENCES

Antia, H. M., & Basu, S. 2000, ApJ, 541, 442

—. 2013, Journal of Physics Conference Series, 440, 012018

Baldner, C. S., & Schou, J. 2012, ApJ, 760, L1

Baldner, C. S., Basu, S., Bogart, R. S., et al. 2013, Sol. Phys., 287, 57

Basu, S., & Antia, H. M. 2010, ApJ, 717, 488

Basu, S., Antia, H. M., & Bogart, R. S. 2004, ApJ, 610, 1157

Basu, S., Antia, H. M., & Tripathy, S. C. 1999, ApJ, 512, 458

Bogart, R. S., Baldner, C., Basu, S., Haber, D. A., & Rabello-Soares, M. C. 2011a, Journal of Physics Conference Series, 271, 012008

—. 2011b, Journal of Physics Conference Series, 271, 012009

Haber, D. A., Hindman, B. W., Toomre, J., et al. 2002, ApJ, 570, 855

—. 2000, Sol. Phys., 192, 335

Hathaway, D. H., Upton, L., & Colegrove, O. 2013, Science, 342, 1217

Hathaway, D. H., Gilman, P. A., Harvey, J. W., et al. 1996, Science, 272, 1306

Hill, F. 1988, ApJ, 333, 996

Howard, R., & Labonte, B. J. 1980, ApJ, 239, L33

Howe, R., Christensen-Dalsgaard, J., Hill, F., et al. 2013, ApJ, 767, L20

—. 2000, ApJ, 533, L163

Komm, R., González Hernández, I., Howe, R., & Hill, F. 2015, Sol. Phys.

Komm, R., Howe, R., González Hernández, I., & Hill, F. 2014, Sol. Phys., 289, 3435

Kosovichev, A. G., & Schou, J. 1997, ApJ, 482, L207

Labonte, B. J., & Howard, R. 1982, Sol. Phys., 80, 361

Patrón, J., González Hernández, I., Chou, D.-Y., et al. 1997, ApJ, 485, 869

Ulrich, R. K. 1998, in ESA Special Publication, Vol. 418, Structure and Dynamics of the Interior of the Sun and Sun-like Stars, ed. S. Korzennik, 851

Ulrich, R. K. 2001, ApJ, 560, 466

Zaatri, A., Komm, R., González Hernández, I., Howe, R., & Corbard, T. 2006, Sol. Phys., 236, 227

Zhao, J., Nagashima, K., Bogart, R. S., Kosovichev, A. G., & Duvall, Jr., T. L. 2012, ApJ, 749, L5